Pairing effects and multistep direct and compound emission in the $^{92-100}$Mo(p,xn) reactions

E. Mordhorst, M. Trabandt, A. Kaminsky, H. Krause, and W. Scobel
I. Institut für Experimentalphysik, Zyklotron, Universität Hamburg, D-2000 Hamburg 50, Federal Republic of Germany

R. Bonetti and F. Crespi
Istituto di Fisica Generale Applicata dell'Università di Milano, Milano, Italy
(Received 21 February 1986)

The reactions ^{92,94,95,96,97,98,100}Mo(p,xn) have been studied with $E_p = 25.6$ MeV protons for neutron angles $3° \leq \Theta_n \leq 177°$. In the preequilibrium region the angle integrated, inclusive neutron energy spectra show pronounced pairing effects that seem to be correlated with the ground state deformation. The angular distributions show more backward yield than predicted by semiclassical preequilibrium models. A quantitative description is obtained with a quantum-mechanical statistical multistep model including three steps of direct and compound plus subsequent equilibrium emission. Both components are calculated consistently with a Yukawa-type residual interaction of strength $V_0 = 25$ MeV.

I. INTRODUCTION

In this paper we study the neutron preequilibrium (PE) emission induced by 25.6 MeV protons from all seven stable molybdenum isotopes. The (p,n) residual nuclei range from $^{92}_{43}$Tc near the $N = 50$ shell closure to $^{100}_{43}$Tc in the new region of deformation[1] at $A \approx 100$, and include odd-odd as well as odd-even nuclei. The neutron time-of-flight experiment has been performed with emphasis on low background measurements covering a broad range of reaction angles (Sec. II). The interpretation of these data focuses on odd-even effects due to pairing correlations and on the angular distributions in the PE continuum as a function of neutron energy and excess (Sec. III A).

Semiclassical PE models that describe a nuclear reaction as proceeding through a sequence of nucleon-nucleon interactions in the nuclear Fermi gas succeed in reproducing average yields and energy spectra of ejectile nucleons. Discrepancies appear whenever considerable residual interactions prevent the usually applied assumption of equidistantly spaced single particle (s.p.) states to be a good one. It has been shown that the grouping of s.p. states near neutron[2] or proton[3] shell closures can be accounted for by using instead realistic s.p. level schemes—in particular for the $1p(1n)^{-1}$ state density of the residual nucleus for a single step interaction. The results of Grimes *et al.*,[4] however, show that for residual systems $\Delta Z = 3$ away from the closed shell $Z = 50$, the effect is significantly reduced, because the shell gap decreases rapidly with increasing deformation and the partial state densities for $Z = 46$—48 change more when *one single* nucleon is added than with the addition of a *pair* of like nucleons. The $^{94}_{40}$Zr(p,n)$^{94}_{41}$Nb data[2] in comparison to those of $^{91}_{40}$Zr(p,n) show a similar reduction in shell irregularities; therefore, the Mo isotopes are good candidates for studying pairing effects in PE emission (Sec. III B).

Nucleon angular distributions for the typical PE region show a strong preference for forward emission. The generalized exciton model in its different versions,[5-8] as well as the geometry dependent hybrid (GDH)[9,10] model reproduce this feature fairly well because they treat the first few intranuclear nucleon-nucleon collisions essentially correctly.[11] However, the backward yield is seriously underestimated in these semiclassical nucleon-nucleon collision models unless the two-body kinematics is treated incorrectly,[8] e.g., by disregarding the energy-angle correlation in averaging over exit channel energies; or additional assumptions concerning refraction,[6,9] or diffraction and the finite nuclear size[5,9] are added *ad hoc*. The latter may also be implemented by evaluating the scattering kernel for bound target nucleon states of a harmonic oscillator potential in plane-wave Born approximation, although this approach[12] leads to unexpectedly high contributions from the later stages of the equilibration. Therefore, a more rigorous quantum mechanical approach in terms of a multistep direct reaction[13,14] seems to be conceptionally preferable.

The quantum statistical model of Feshbach *et al.*[14] makes a distinction between the multistep direct emission (SMDE) proceeding through states with unbound particles and the statistical multistep compound emission (SMCE) involving only particle bound states. This model works well not only under conditions leading to a dominance of the SMDE (Ref. 15) or the SMCE (Ref. 16) process, but also in single cases [^{120}Sn(p,n),[17] ^{65}Cu(p,n) (Ref. 18)] for medium energies $E_p \approx 25$ MeV where both mechanisms contribute with comparable intensity. These analyses converge[17,19] towards a unique parameter set that, so far, has never undergone a systematic test against a sequence of targets, allowing one to study the trends with increasing neutron excess in yield as well as in angular shape. In Sec. III C we present such a test with $^{92-100}$Mo. Finally, our conclusions are summarized in Sec. IV.

II. APPARATUS AND MEASUREMENT

The experiment has been carried out at the Hamburg Isochronous Cyclotron with 25.6 MeV protons and a neu-

tron time-of-flight (TOF) array of eight detectors designed for low background and large angular range.[20]

The proton beam can be focused onto one of three subsequent target positions in a reaction chamber with a shape corresponding to a 34° segment of a circle. Two magnets with C yokes of gap width 10 cm between the target positions each bend the beam by 17° such that it passes through the chamber and is dumped into a heavily shielded Faraday cup.

Reaction neutrons from the target position in operation enter flight paths of (7.5±0.5) m length through a thin exit window towards the neutron detectors. The detectors consist of cylindrical 10 cmϕ×5 cm cells filled with liquid scintillator NE213 and coupled to photomultipliers VALVO XP2041. They view the targets through collimator tubes traversing water shielding of more than 1 m thickness. Conical polyethylene throats at the front ends of the collimator tubes supplement the efficient shielding against time correlated and stray neutrons. The collimator tubes can be aligned towards any of the three optional target positions such that the setup covers an interval of reaction angles Θ ranging from 3° to 177° with 24 fixed positions and increments of 6.5° for small and large, and 10.5° for intermediate angles, respectively.

The TOF electronics are conventional. Low energy biases $E_{n,thr}=0.9-1.1$ MeV were applied to guarantee an effective n-γ discrimination. The TOF stop signal was derived from the cyclotron radio frequency; the burst frequency was scaled down to ≈ 1.4 MHz by means of an external deflector. The overall time resolution obtained was ≈ 1.5 ns (FWHM) corresponding to a neutron energy resolution of 60 keV (500 keV) for $E_n=5$ MeV (20 MeV).

Measurements were performed for all seven stable molybdenum isotopes; target specifications, maximum neutron energies in the c.m. system and charges accumulated are listed in Table I. Each primary run was followed by a shorter background run with shadow bars placed in the flight paths about midway between target and detectors. The background subtraction represented at most a 10% correction of the integral yield in the physical region $E_{n,thr} \le E_n \le E_{n,max}$ and was substantial ($\le 20\%$) only for the extreme backward angles and high neutron energies. Further experimental details have been reported elsewhere.[18,20]

Neutron energy spectra in the c.m. system were obtained by application of detector efficiencies as calculated with the code NEFF4 (Ref. 21) and kinematic transformations assuming single neutron emission.

Relative uncertainties between neutron spectra obtained in different runs are mostly due to target thickness inhomogeneity (5%), inconsistencies in the background treatment (5%), and incomplete beam current integration (3%). The estimated uncertainty is 10% for all angles and all but the highest neutron energies. Absolute uncertainties are slightly higher due to the uncertainty in the efficiency calculations ($\le 5\%$). We estimate absolute un-

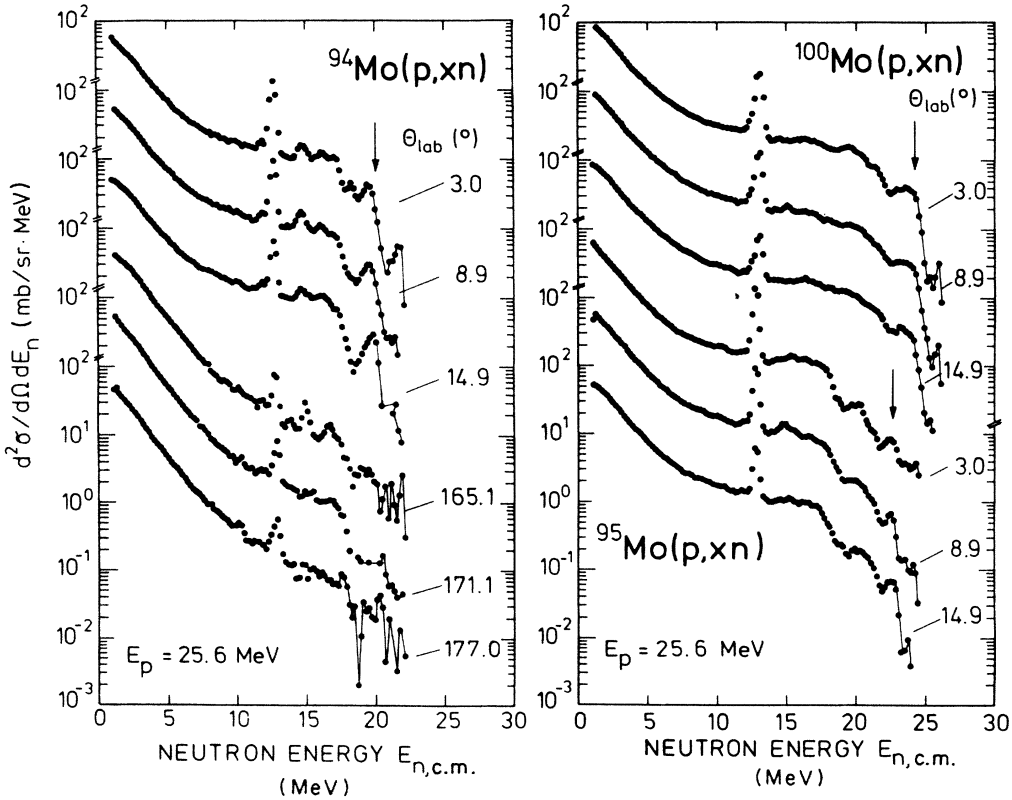

FIG. 1. Representative spectra obtained for ^{94,95,100}Mo(p,xn) under several angles. The arrows indicate the ground state transitions.

TABLE I. Target and reaction data.

Target	Enrichment (%)	Thickness (mg/cm^2)	Q(p,n) (MeV)	$E^{c.m.}_{n,max}$ (MeV)	Charge accumulated (mC)
^{92}Mo	98.5	3.79	−8.65	16.5	1.1–1.2
^{94}Mo	94.6	2.64	−5.04	20.1	0.8–1.0
^{95}Mo	97.4	4.18	−2.47	22.6	0.8–1.0
^{96}Mo	97.7	4.31	−3.76	21.4	0.8–1.0
^{97}Mo	94.3	4.65	−1.10	24.0	0.9–1.0
^{98}Mo	98.8	4.16	−2.47	22.6	0.8–0.9
^{100}Mo	98.0	4.15	−0.95	24.2	0.7–0.8

certainties $\lesssim 12\%$ for most of the double differential and all angle integrated cross sections.

III. RESULTS AND DISCUSSION

A. Experimental results

A subset of the angle differential energy spectra for ^{94,95,100}Mo(p,xn) is shown in Fig. 1. The data are statistically significant down to the 10^{-2} mb/sr MeV level. The width of the isobaric-analog state (IAS) corresponds to the energy resolution; the experiment was not designed to resolve the excited analog states.

The structures observed in the spectra for $U < 6$ MeV are correlated in angle for each isotope. They have been interpreted in Refs. 2 and 22 to result from the individual $1p(1n)^{-1}$ state density of the residual nuclei near the shell closure $N = 50$. This applies to $^{94}_{43}$Tc, to a lesser extent to $^{95}_{43}$Tc, and not at all to $^{100}_{43}$Tc. In comparing the structures we note the following differences and similarities between the isotopes:

(i) The spectra extend to the high energy limit for ^{100}Mo, whereas they show a moderate gap Δ above the ground state (g.s.) transition for ^{94}Mo, ^{95}Mo, and ^{97}Mo.

(ii) The structures are pronounced for ^{94}Mo→^{94}Tc and ^{95}Mo→^{95}Tc, but are more or less smoothed out for ^{100}Tc although the experimental conditions remained the same.

(iii) The angular distribution of a given neutron energy bin $(E_n, E_n + \Delta E_n)$ in the continuum region seems to be essentially independent of the isotope; the descent from 0° to 180° visible in Fig. 1, e.g., at $E_n \approx 15$ MeV corresponds to a factor of 10 and is lower (higher) with decreasing (increasing) E_n.

Observations (i) and (ii) will be discussed further in terms of pairing effects and the influence of g.s. deformation in Sec. III B, whereas the discussion of angular distributions is presented in Secs. III C and III D.

B. Pairing and preequilibrium emission

Pairing effects should become more pronounced in the angle integrated spectra. Figure 2 shows the result of this work in comparison with the data of Ref. 22 taken at

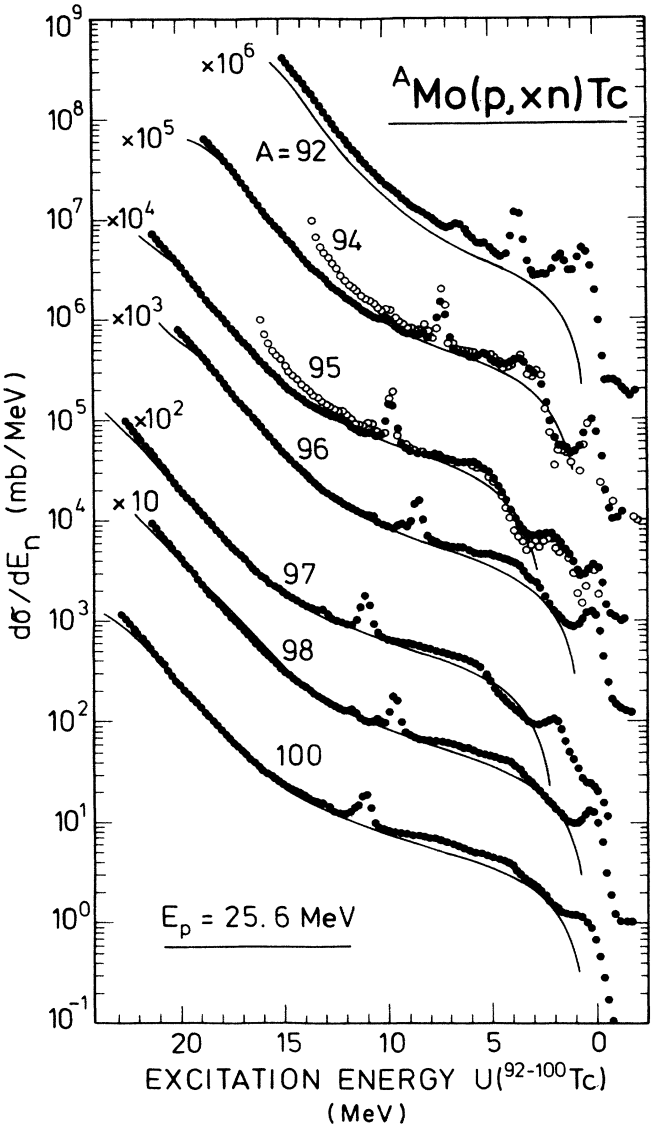

FIG. 2. Angle integrated neutron energy spectra of this work (solid dots) and of Ref. 22. The solid lines denote the GDH plus evaporation model calculations applying the pairing shifts $\Delta(\delta)$ of Table II.

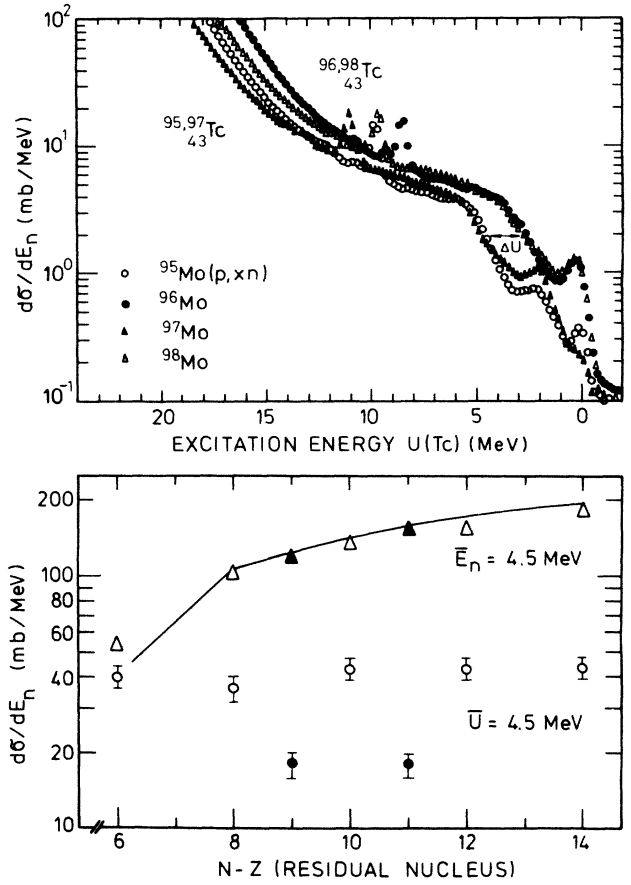

FIG. 3. Top: Angle integrated spectra for $^{95-98}$Mo(p,xn) vs residual excitation in $^{95-98}$Tc, running from right to left. Bottom: Experimental cross sections $d\sigma/dE_n$ for $\bar{E}_n$=4.5 MeV and $\bar{U}$=4.5 MeV, respectively; filled symbols indicate odd-odd residual nuclei. The line connects cross sections $d\sigma(\bar{E}_n)/dE_n$ calculated (Ref. 36) with pairing corrections.

E_p=25.0 MeV. The latter data show better energy resolution than ours due to the longer flight path (11 m vs 7.5 m); the discrepancies at lower neutron energies E_n (or, higher residual excitation energies U) can be traced back to the different threshold (thr) energies $E_{n,thr}$ and efficiencies applied. The agreement in the region between the IAS and the g.s. transition where PE emission dominates, indicates that the structures are not affected by the difference $\Delta E_p \approx 0.6$ MeV in projectile energies; they are therefore correlated with the residual excitation. The model calculations shown will be referred to later on.

The influence of the odd-odd or odd-even character of the residual nucleus is obvious from Fig. 3 where the angle integrated spectra for $^{95,96,97,98}_{42}$Mo(p,n)Tc are plotted on top of each other. For the odd-odd nuclei $^{96,97}_{43}$Tc the spectra are very similar; the same applies to those of the odd-even nuclei $^{95,97}_{43}$Tc. However, the continuous part of the spectrum is shifted by $\Delta U \approx 2$ MeV to higher excitation U. The lower part of Fig. 3 shows that this trend continues over the whole mass range $^{92-100}_{43}$Tc, whereas it is barely visible in the typical evaporation region $\bar{E}_n$=4.5 MeV. It should therefore find its explanation from the phase space allocated to transitions leading into this part of the continuous spectrum.

Semiclassical phase space models for preequilibrium emission predict the nucleon energy spectra from nucleon induced reactions to be [23] given by

$$\frac{d\sigma(\epsilon_\nu)}{d\epsilon_\nu} = \sigma_R \sum_{n=3}^{\bar{n}} D_n g \frac{\rho_{p-1,h}(U)}{\rho_n(E)} \lambda_c(\epsilon_\nu) t(n,\epsilon_\nu,E) \ . \quad (1)$$

Here, σ_R is the reaction cross section for formation of the composite system at excitation energy E. The sum extends over contributions of stages characterized by the exciton number $n=p$ (particles)$+h$ (holes); λ_c is the decay rate for the continuum emission of neutrons (ν) with energy ϵ_ν, and D_n the depletion due to this emission from preceding stages $n' < n$. The models differ in the lifetime expression $t(n,\epsilon_\nu,E)$ as well as in the conceptional treatment of intrinsic configuration mixing.[24] The quantity ρ_x denotes the density of states with the exciton configuration x at the excitation E (U) of the composite (residual) system.

Due to the dominance of the leading term in the sum, the dependence of the spectrum, Eq. (1), on ϵ_ν is given in first order by

$$\frac{d\sigma(\epsilon_\nu)}{d\epsilon_\nu} \sim \rho_{1,1}(U) \ , \quad (2)$$

For (p,n) reactions, the right-hand side is the density of the one proton-particle, one neutron-hole, or $1p(1n)^{-1}$, states in the residual nucleus.

In the Fermi gas model with equidistant spacing g^{-1}, the partial density of n exciton states composed of p particles and h holes is given by[25]

$$\rho_{p,h}(U) = g \frac{[g(U-A)]^{n-1}}{p!h!(n-1)!} \ , \quad (3)$$

i.e., a smooth function of U that extends to the ground state at $U=0$. The correction A accounting for the Pauli exclusion principle vanishes for the $1p1h$ state density, such that $\rho_{1,1}(U)=g^2U$.

However, a calculation of the spectra with Eqs. (2) and (3) is at variance with the experimental results in Fig. 2. Residual interactions not properly taken into account by Eq. (3) must be responsible for the deviation from the smooth phase space behavior. It has been shown in Refs. 2 and 3 that the influence of a nearby shell closure as well as the pairing of nucleons can be taken care of by generating $\rho_{1,1}$ out of a given set of realistic s.p. states of a Nilsson model description (with given N, Z, and deformation δ). The pairing effect is included in terms of the Bardeen-Cooper-Schrieffer (BCS) formalism[26] with quasiparticle energies, whose gap parameters Δ_0 were taken to be equal to the pairing energies of Gilbert and Cameron.[27]

Figure 4 shows calculations of this type for ^{94}Tc as a spherical nucleus ($\delta=0$) as well as for moderate ($\delta=0.1$) deformation. The state density according to Eq. (3) with $g=\frac{1}{2}(6/\pi^2)a$ and the level density parameter $a=A/8$ MeV^{-1} is shown, too, as well as the experimental spectrum normalized with 1 mb/MeV to 1 level/100 keV.

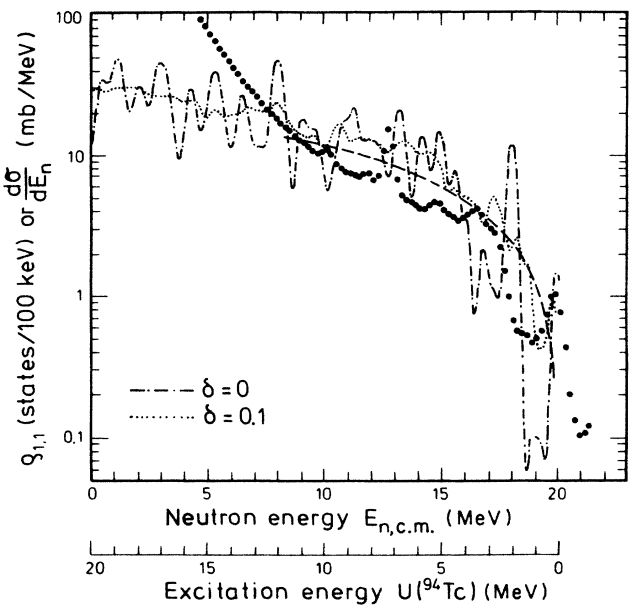

FIG. 4. Two quasiparticle densities $\rho_{1,1}$ generated with s.p. levels of Ref. 29 for ($\delta=0$) spherical and ($\delta=0.1$) deformed ^{94}Tc after smoothing (Ref. 2) with $\sigma=1.5$ MeV. The result of Eq. (3) (dashed line) and the arbitrarily normalized spectrum for ^{94}Mo(p,n)^{94}Tc (circles) are shown, too.

Recently, Fu[28] has shown that pairing can be included in the partial state densities of Ref. 25 by replacing in Eq. (3) $U-A$ by $U-B(n,\Delta_0)-P(n,U)$. The quantity $B(n,\Delta_0)$ corrects the Pauli correction A for nonuniform s.p. spacing of quasiparticle energies in the case of pairing with a gap parameter Δ_0; however, it is $B\sim A$, and therefore B vanishes for $1p1n^{-1}$ states. In the pairing correction term

$$P(n,U)=\tfrac{1}{4}g[\Delta_0^2-\Delta^2(U,n)]\,, \tag{4}$$

the quantity $\Delta(U,n)$ denotes the pairing gap in a state of excitation U and exciton number n. Inspection of $\Delta(U,n)$ leads[28] to the conclusion that $P(n,U)$ may be replaced by a *constant* pairing energy shift, if the calculated cross section is sensitive to essentially only one exciton number preferentially $n=2$. This is exactly the situation we are facing with Eq. (2). This constant value is expected to range from $\frac{1}{4}g\Delta_0^2$ (if pairing correlations are totally broken at excitation U) and 0 (if $\Delta\equiv\Delta_0$, i.e., the pairing correlations are not at all blocked) as long as the underlying assumption of equidistant spacing in the absence of pairing is essentially correct. For our residual nuclei $^{95,97}_{43}$Tc, $g\approx 6.4$ MeV^{-1} (corresponding to $a\approx A/9$ MeV^{-1}) and $\Delta_0\approx 1.1$ MeV,[27] the calculation[28] yields $\Delta/\Delta_0\approx 0.6$ or $P\approx 1.2$ MeV for $1p1h$ states at lowest possible[26,28] excitation $U_{\rm thr}\approx 1.9$ MeV. For the residual Tc nuclei with even mass number, we anticipate $P\approx 0$. We have performed calculations with this pairing treatment in the framework of the geometry dependent hybrid (GDH) plus Ewing-Weisskopf model[36] and found less, but still some, disagreement. We doubt that shell effects can be made responsible for the remaining differences, because for $^{95-98}_{43}$Tc the nucleon numbers exceed (with one exception) shell closures by at least three units and the shell irregularities (visible, e.g., in Fig. 4) tend to wash out as mentioned before.[2,4] Instead, the nuclear deformation may lead to deviations from the uniform spacing of s.p. states in a way equivalent to a decrease of the effective excitation energy $U_{\rm eff}$.

In order to account for a possible deformation contribution to a shift of U to $U_{\rm eff}=U-P$, we replaced the uniformly spaced s.p. states by realistic Nilsson model s.p. states for different deformations $0\le\delta\le 0.3$, based on the parameters of Seeger and Howard.[29] The $1p(1n)^{-1}$ state density was generated from this set of s.p. states as outlined in Ref. 2. The resulting state densities were expressed as $\rho_{1,1}(U)=g^2[U-\Delta(\delta)]$ with best fitting values g and $\Delta(\delta)$ for residual excitations up to 10 MeV. These values were then inserted into a GDH model[36] calculation. The best fits are shown in Fig. 2; they were obtained with the values $\Delta(\delta)$ listed in Table II that belong to the deformations shown in Fig. 5. The deformation values are uncertain to within ± 0.05. They do not seem to be unrealistic when compared with calculations[30] of spin zero potential energy surfaces within the cranked Nilsson-Strutinsky model, including pairing for the adjacent Mo and Ru isotopes, or with the recent results[1,31] for $^{103-105}$Mo. Their monotonic increase with neutron excess leads to Nilsson s.p. level schemes that come closer to a uniform spacing. As a consequence the structures in the experimental spectra should diminish as observed [cf. Fig. 2 and (ii) in Sec. III A].

The shifts $\Delta(\delta)$ are higher than expected according to Fu.[28] They also differ from those of Gilbert and Cameron[27] and of the back shifted Fermi gas model[39] that are in use for equilibrium emission calculations. This may be partly due to the fact that $\rho_{p,h}(U)$ of Eq. (3) needs a renormalization[40] before it can be compared with state density expressions for Hauser-Feshbach calculations like the one of Ref. 39. Akkermans and Gruppelaar[40] also point out that Eq. (3) tends to be incorrect at low excitation due to deviations from equal spacing. Our values $\Delta(\delta)$ may

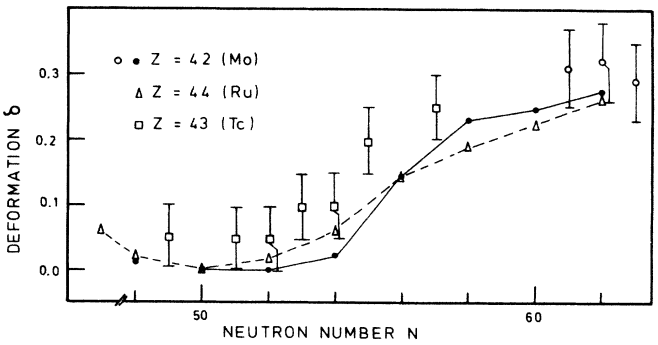

FIG. 5. Nuclear deformations δ vs neutron number N. Calculated values (Ref. 30) for Mo and Ru are connected by lines, open circles are experimental values (Refs. 1 and 31). The δ values for Tc are those of the best fitting shifts $\Delta(\delta)$ listed in Table II.

TABLE II. Pairing corrections $\Delta(\delta)$ (in MeV) for deformed residual nuclei $^{92-100}$Tc reached by PE emission; compared with Δ_0 from Ref. 27 and Δ_D (extrapolated from Ref. 39).

Residual nucleus	^{92}Tc	^{94}Tc	^{95}Tc	^{96}Tc	^{97}Tc	^{98}Tc	^{100}Tc
Δ_0	0	0	0.72	0	1.12	0	0
$\Delta(\delta)$	0.66	1.06	2.76	1.03	2.27	0.77	0.60
Δ_D	−0.8	−0.8	+0.2	−0.8	+0.2	−0.8	−0.9

therefore be considered an additional[2] indication for the sensitivity of (p,n) preequilibrium emission to the details of the residual interaction not taken care of with phase space expressions.

C. Angular distributions: Trends

In contrast to the neutron energy distributions and yields, the angular distributions are not supposed to strongly depend on the target-projectile combination. The main argument is that the general extent of agreement between preequilibrium decay models—irrespective of their differences in physical grounds and formal structure[24]—and experimental data can be traced back[11] to the dominance of the first (and second) hierarchy of nucleon-nucleon interactions. Nucleon angular distributions therefore reflect the pattern of intranuclear nucleon-nucleon scattering in one- or two-step processes folded over a range of relative energies, plus contributions from processes of the equilibrated reaction system. The range of relative energies contributing is dependent on the exit channel energy ϵ_n; the phenomenological parametrization of nucleon angular distributions in PE processes in terms of coefficients that depend only on ϵ_n takes advantage of this[32] gross behavior.

It has been amply discussed in Ref. 9 that in the mass and energy range under consideration semiclassical PE models fail more or less for angles close to 0° and 180°, whereas quantum mechanical and quantum statistical models can do better, in particular at the crucial backward angles. The model of Feshbach, Kerman, and Koonin[14,33] has been proven[17,18] successful in the region of energies where both SMDE and SMCE contribute with comparable yields. We shall, after giving next an account of the trends related to neutron energy and neutron excess, summarize in short this model and then compare the predictions of this model with our data in Sec. III D.

For convenience we describe our angular distributions in terms of the best fitting Legendre polynomial expression for each target isotope A

$$\frac{d^2\sigma(\Theta_n)}{d\Omega\, d\epsilon_n} = \sum_{\nu=0}^{\nu_{max}} a_\nu(\epsilon_n, A) P_\nu(\cos\Theta_n) \tag{5}$$

extending to $\nu_{max}=4$. The coefficients $a_0(\epsilon_n, A)$ and therefore the yields $4\pi a_0$ increase smoothly with A for low energies ϵ_n and show an odd-even pattern for higher energies (cf. Fig. 3). Focusing on the *shape* of the angular distributions, we restrict the discussion to the reduced coefficients

$$b_\nu(\epsilon_n, A) = a_\nu(\epsilon_n, A)/a_0(\epsilon_n, A)\ .$$

These coefficients are shown in Fig. 6(a) for ^{100}Mo(p,xn). Their smooth energy dependence is obvious; it is only interrupted at the ground state transition and the isobaric analog resonance, respectively. Figure 6(b) confirms that the angular distributions do indeed have a shape that is in the region of dominant nonequilibrium processes, within the uncertainties stated, not dependent on the neutron excess. ^{92}Mo is not included because the spectrum extends only to $E_n = 16.5$ MeV.

The phenomenological parametrization of Ref. 32 is shown in Fig. 6(b), too. It is essentially correct for b_1, but underestimates the contributions represented by Legendre polynomials of higher order. This is probably due to the under-representations of neutron and backward angle data in the data basis of that compilation.

D. Statistical multistep calculations

The model of Feshbach *et al.* has been described in detail elsewhere.[15,16,23] Here, we quote only the basic formulas necessary to explain the input to our calculations. For more details the reader is referred to our ^{65}Cu(p,n) paper,[18] because the present calculations of double differential cross sections for $^{94-100}$Mo(p,n) at several ejectile energies and angles have been performed exactly in the same way.

For the SMCE process, the cross section is given by

$$\frac{d^2\sigma}{dU\, d\Omega} = \sum \frac{(-1)^{s'-s}}{(2I+1)(2i+1)} \bar{Z}(lJlJ;sL)\bar{Z}(l'Jl'J;sL) P_l(\cos\Theta) \times \frac{\pi}{k^2} \sum_{n=1}^{r} \sum_{\nu=n-1}^{n+1} \frac{\langle \rho_{\gamma\nu}(U)\Gamma_n^{(\gamma\nu)}(U)\rangle}{\Gamma_n} \left[\prod_{k=1}^{n-1} \frac{\Gamma_k^{\downarrow}}{\Gamma_k}\right] \frac{2\pi\Gamma_1}{D_1}\ . \tag{6}$$

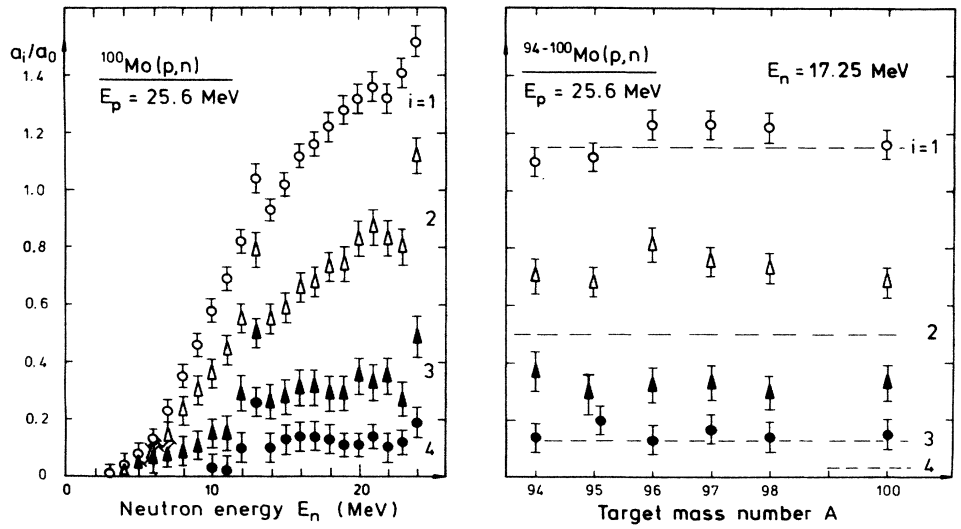

FIG. 6. Reduced coefficients a_i/a_0 of Eq. (5) fitted to the angular distributions of ^{100}Mo(p,xn) for different ejectile energies E_n, and for $^{94-100}$Mo and $E_n = 17.25 \pm 0.25$ MeV as a function of target mass number A. Dashed horizontal lines denote the values of Ref. 32.

Herein, the strength function $2\pi\Gamma_1/D_1$, the damping ($\Gamma_k^{\downarrow}$), and the escape ($\Gamma_n^{\gamma\nu}$) widths were calculated with matrix elements of the residual nucleon-nucleon interaction evaluated with realistic wave functions: The initial and final distorted waves were derived with an optical model potential and neutron (proton) parameters of Wilmore and Hodgson[34] (Becchetti and Greenlees[35]); both parameter sets scale with neutron excess $N-Z$. The bound state shell-model wave functions are based on a simple harmonic oscillator potential.

Only single particle emission was considered during the equilibration stage. Due to the moderate projectile energy, multiple emission represents only a small contribution[18,36] for ejectile energies above ~ 10 MeV. All level densities were calculated with level density parameters a increasing with target mass number from 15 to 16 MeV^{-1}. Pairing was taken care of by replacing the residual excitation U by the effective value $U-\Delta_0$ for the residual nuclei ^{95,97}Tc; the pairing energies Δ_0 were taken from Ref. 27. The spin cutoff parameter σ in the angular momentum dependence of the level density was set to 1.5. Spins of incoming and outgoing particles, respectively, were disregarded.

For the SMDE process, the cross sections were calculated from

$$\frac{d^2\sigma}{dU\,d\Omega} = \sum_{\nu} \sum_{m=n-1}^{n+1} \int \frac{d\mathbf{k}_1}{(2\pi)^3} \cdots \int \frac{d\mathbf{k}_\nu}{(2\pi)^3} \left[\frac{dW_{m,\nu}(\mathbf{k}_f,\mathbf{k}_\nu)}{dU_f d\Omega_f} \right] \left[\frac{dW_{\nu,\nu-1}(\mathbf{k}_\nu,\mathbf{k}_{\nu-1})}{dU_\nu d\Omega_\nu} \right] \cdots \times \left[\frac{dW_{2,1}(\mathbf{k}_2,\mathbf{k}_1)}{dU_2 d\Omega_2} \right] \frac{d^2\sigma_{1i}(\mathbf{k}_1,\mathbf{k}_i)}{dU_1 d\Omega_1} , \tag{7}$$

with

$$\frac{d^2\sigma_{1i}}{dU_1 d\Omega_1} = \sum_L (2L+1) R_2(L) \rho_2(U) \left\langle \frac{d\sigma_L^{(\mathrm{DW})}}{d\Omega} \right\rangle \tag{8}$$

and

$$\frac{dW_{n,n-1}}{dU\,d\Omega} = 2\pi^2 \rho(k) \rho_2(U) \, |\, v_{n,n-1} \,|^2 . \tag{9}$$

All distorted waves have been computed with the same optical model potentials, and the $1p\,1h$ level density $\rho_2(U)$ was based on the same parameter values a as for the SMCE part. The bound state wave functions were generated in a Woods-Saxon potential with radius parameter $r_0 = 1.3$ fm and diffusity of 0.7 fm.

The residual nucleon-nucleon interaction has been given a Yukawa shape of 1.0 fm range and strength V_0 of 25 MeV. This strength is only slightly lower than the value $V_0 \approx 27$ MeV obtained in Refs. 15 and 19 and confirmed in Ref. 18. The calculations have been extended up to the third step for SMDE. The SMCE component, in addition to these three steps, also contains the contributions of the compound nucleus r stage. The transition from SMCE to evaporation is fixed by a condition imposed on the saturation of the exciton level density with increasing exciton number.[14]

The relative contributions of the SMDE and SMCE process depend on ejectile energy as well as on the angle. Figure 7 shows for two representative angles and the ^{100}Mo(p,n) reaction, that SMDE is forward directed and exceeds (for $\Theta = 15°$) the SMCE at high neutron energies by one order of magnitude, whereas under backward angles ($\Theta = 134°$) the SMCE, due to its almost isotropic emission characteristics, contributes substantially at all but the highest energies E_n. The r-stage contributions to the SMCE are small for all neutron energies under consideration (cf. Fig. 7), smaller than those of Ref. 16 which were obtained at 16–18 MeV projectile energy. This is a consequence of the small depletion factor for r-stage processes due to the relatively high incident energy $E_p \approx 25$ MeV, favoring high energy precompound neutron emission. The calculation shows, indeed, that less than 10% of the incoming flux going to the bound states is available for the evaporation process.

We shall next have a closer look at the dependence of the two processes on E_n and Θ by comparing the angular distributions for the energy bins indicated in Fig. 7 by the position and width of the four arrows. The highest energy bin 21.75 ± 0.25 MeV in Fig. 8 corresponds to an excitation energy $U = 2.4$ MeV in odd-odd nucleus $^{100}_{43}$Tc; its angular distribution descends by a factor of 20 from $\Theta = 0°$ to 180° and so does the SMDE component, which is almost identical with the first step contribution. The SMCE contribution is negligibly small even at backward angles (cf. Fig. 7) and therefore not included. The SMDE oscillations at backward angles are directly related to the details of the radial DWBA form factor and therefore to the choice of the bound state parameters and the range of the interaction. Better fits might be obtainable by parameter variation, but we did not intend to optimize these fits provided that the general features were well reproduced by the present multistep calculation.

At $E_n = 17$ MeV, the first step SMDE contribution is not sufficient for explaining the experimental data; the second and third step contributions are of similar size, but much more isotropic, and therefore enhance the angular distribution at backward angles. The SMCE contribution starts to show up at backward angles. This trend continues to lower neutron energies, and at $E_n = 9.5$ MeV the SMDE is not sufficient to explain the angular distribution, and only addition of the isotropic SMCE component leads to a quantitative reproduction of the experimental data.

It has been discussed earlier in this paper that the shape of the angular distributions shows only little, if any dependence on the neutron excess. This statement has been quantified in Fig. 6(b) for the $E_n = 17.0$ MeV data. Figure 9 shows that the SMDE plus SMCE calculations reproduce this feature very well. The shape of the angular distribution is in all cases essentially determined by the first two or three steps of the SMDE process in agreement with Ref. 11. The absolute values scale correctly with neutron excess by a factor of ≈ 1.5 from ^{94}Mo to ^{100}Mo. The contributions of the more isotropic processes (second and higher steps SMDE and SMCE) are seen to increase from ^{94}Mo to ^{100}Mo. The increase exceeds that of this first step SMDE plus SMCE process. This trend is well known, e.g., from (p,xn) and, with opposite sign, from (p,xp) reactions on Ni and Cu isotopes,[37] and is related there to the increasing energetic preference of *(multiple)* nucleon emission [cf. also Fig. 3(b)]. Figure 9 shows this trend already for 17 MeV neutrons, i.e., for *single* neutron emission reflecting the decrease of the (p,n) Q value (Table I).

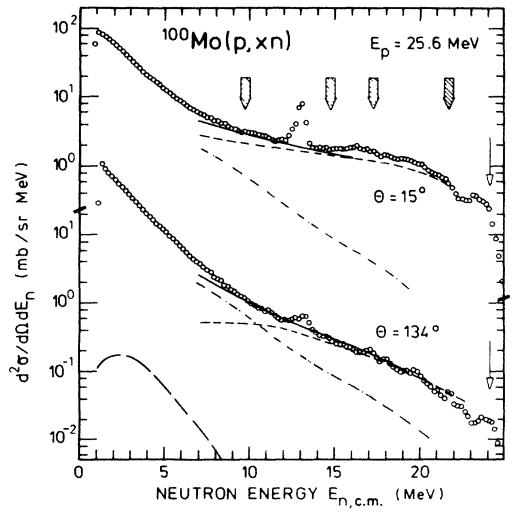

FIG. 7. Experimental neutron energy spectra (circles) for p+^{100}Mo in comparison with SMDE (dashed line) and SMCE (dash-double dot) calculation and the sum (solid line). The long dashed line denotes the mere r-stage component (single particle evaporation only).

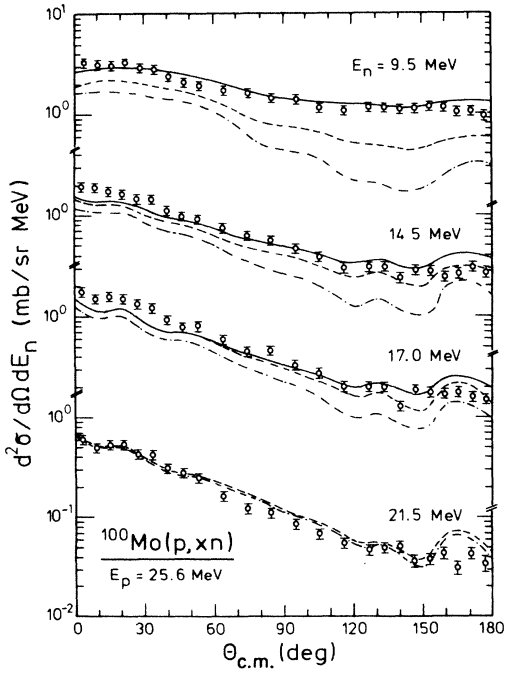

FIG. 8. Experimental angular distributions (circles) of neutrons from ^{100}Mo(p,xn) for the bins (E_n,E_n+0.5 MeV). Calculations are first step SMDE (dash-dotted line), SMDE of the first three steps (dashed), and the sum SMDE plus SMCE (solid line).

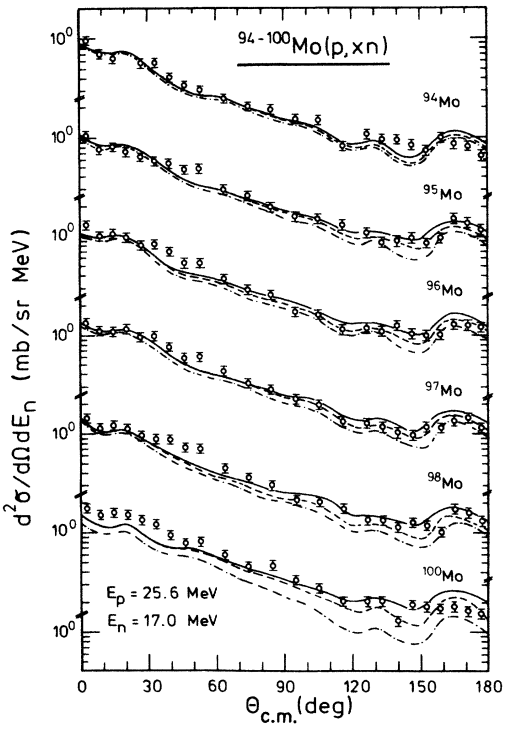

FIG. 9. Angular distributions of neutrons from $^{94-100}$Mo(p,xn) for the bin 17.0—17.5 MeV. See Fig. 8 for explanation of symbols.

Finally we emphasize that these results are in agreement with those of the (p,n) reactions on ^{120}Sn (Ref. 17) and ^{65}Cu (Ref. 18) with 25 MeV protons. The same set of parameters has been used in all cases; in particular the residual nucleon-nucleon interaction has been given a strength $V_0 \approx 25$—27 MeV for both, SMCE and SMDE processes. This value is in agreement with the average strength $V_{\text{eff}} = 27.9 \pm 3.5$ MeV of the empirical effective interaction obtained from DWBA fits to inelastic proton scattering data in the $E_p = 20$—50 MeV region.[38] In this sense there is no adjustable parameter in these calculations. The competition between the SMDE and SMCE process can probably be studied more effectively with lower projectile energies (18—20 MeV, see Ref. 16), because then the isotropic nonevaporation component due to excitation of particle bound states should show up even more clearly.

IV. CONCLUSIONS

The inclusive, double differential cross sections $d^2\sigma/d\Omega\, dE_n$ for $^{92-100}_{42}$Mo(p,xn)$^{92-100}_{43}$Tc presented in this work result in angle integrated energy spectra that show a clear odd-even pattern if compared to two or more mass units away from the shell closure $N = 50$. The pairing energies Δ necessary for their description in the framework of the geometry dependent hybrid model are larger than those in use for equilibrated systems. They can be correlated with a nuclear deformation parameter δ necessary to generate Δ from a set of realistic Nilsson model s.p. states for the partial state density $\rho_{1,1}$ in the leading term of the preequilibrium model.

The shapes of the angular distributions in the continuum depend smoothly on the ejectile energy E_n, but do not vary with neutron excess $N-Z$ of the residual nucleus. They are well described by the quantitative multistep compound and direct theories, which have definitely proven to work well also in these "medium" energy cases.

At high neutron energies the reactions are dominated by the 1—3 step direct mechanism that the forward directed angular distributions are indicative of; compoundlike processes, however, contribute more significantly with increasing residual excitation energy. This is of course due to the decrease of the average excitation energy available per exciton that favors the population of bound states. Competition between the two mechanisms is best seen in the calculations for ^{100}Mo(p,xn) at $E_n = 9.5$ MeV, where both, SMCE and SMDE contribute with comparable yield.

The value $V_0 = 25$ MeV for the strength of the residual interaction of Yukawa shape with finite range is in agreement with previous results for pure SMCE and SMDE as well as DWBA calculations. From this point of view the theory of Feshbach, Kerman, and Koonin seems to provide a consistent transition from direct to equilibrium reactions without any discontinuity in parametrization.

This work was supported by the Bundesministerium für Forschung und Technologie, and by the Instituto Nazionale di Fisica Nucleare, Sezione di Milano.

[1]T. Seo, H. Lawin, G. Lhersonneau, R. A. Meyer, G. Menzen, and K. Sistemich, Z. Phys. A **320**, 393 (1985).
[2]W. Scobel, M. Blann, T. T. Komoto, M. Trabandt, S. M. Grimes, L. F. Hansen, C. Wong, and B. A. Pohl, Phys. Rev. C **30**, 1480 (1984).
[3]M. Blann, S. M. Grimes, L. F. Hansen, T. T. Komoto, B. A. Pohl, W. Scobel, M. Trabandt, and C. Wong, Phys. Rev. C **32**, 411 (1985).
[4]S. M. Grimes, J. D. Anderson, and C. Wong, Phys. Rev. C **13**, 2224 (1976).
[5]G. Mantzouranis, H. A. Weidenmüller, and D. Agassi, Z. Phys. A **276**, 145 (1976).
[6]C. Costa, H. Gruppelaar, and J. M. Akkermans, Phys. Rev. C **28**, 587 (1983).
[7]S. Ziyang, W. Shunuan, Z. Jingshang, and Z. Yizhong, Z. Phys. A **305**, 61 (1982).
[8]A. Iwamoto and K. Harada, Nucl. Phys. **A419**, 472 (1984).
[9]M. Blann, W. Scobel, and E. Plechaty, Phys. Rev. C **30**, 1493 (1984).
[10]G. Mantzouranis, Phys. Lett. **63B**, 25 (1976).
[11]H. C. Chiang and J. Hüfner, Nucl. Phys. **A349**, 466 (1980).
[12]K. Sato, Phys. Rev. C **32** 647 (1985).
[13]T. Tamura, T. Udagawa, and H. Lenske, Phys. Rev. C **26**, 379 (1982).

[14]H. Feshbach, A. Kerman, and S. Koonin, Ann. Phys. (N.Y.) **125**, 429 (1980).
[15]R. Bonetti, M. Camnasio, L. Colli-Milazzo, and P. E. Hodgson, Phys. Rev. C **24**, 71 (1981).
[16]R. Bonetti, L. Colli-Milazzo, and M. Melanotte, Phys. Rev. C **27**, 1003 (1983).
[17]R. Bonetti and L. Colli-Milazzo, *Proceedings of the Workshop on Coincident Particle Emission from Continuum States (COPECOS),* edited by H. Machner and P. Jahn (World Scientific, Singapore, 1984), p. 174.
[18]Y. Holler, A. Kaminsky, R. Langkau, W. Scobel, M. Trabandt, and R. Bonetti, Nucl. Phys. **A442**, 79 (1985).
[19]R. Bonetti and L. Colombo, Phys. Rev. C **28**, 980 (1983).
[20]Y. Holler, A. Kaminsky, B. Scharlemann, H. Krause, R. Langkau, W. Peters, G. Poppe, N. Schirm, W. Scobel, and R. Wien, Nucl. Instrum. Methods **A235**, 123 (1985).
[21]G. Dietze and H. Klein, Report PTB-ND-22 (Physikalisch-Technische Bundesanstalt, Braunschweig, 1982).
[22]M. Blann, L. F. Hansen, T. T. Komoto, B. A. Pohl, C. Wong, S. M. Grimes, Y. Holler, W. Scobel, and M. Trabandt, *Proceedings of the International Workshop COPECOS,* edited by H. Machner and P. Jahn (World Scientific, Singapore, 1984), p. 46.
[23]J. Ernst and J. Rama Rao, Z. Phys. A **281**, 129 (1977).
[24]J. Bisplinghoff, Phys. Rev. C, in press.
[25]F. C. Williams, Nucl. Phys. **A166**, 231 (1971).
[26]L. G. Moretto, Nucl. Phys. **A243**, 77 (1975).
[27]A. Gilbert and A. G. W. Cameron, Can. J. Phys. **43**, 1446 (1965).
[28]C. Y. Fu, Nucl. Sci. Eng. **86**, 344 (1984).
[29]P. A. Seeger and W. M. Howard, Nucl. Phys. **A238**, 491 (1975).
[30]S. Åberg, Phys. Scr. **25**, 23 (1982).
[31]K. Sistemich, B. D. Kern, W. D. Laupe, H. Lawin, and H. Seyfarth, Z. Phys. A **289**, 225 (1979).
[32]C. Kalbach and F. M. Mann, Phys. Rev. C **23**, 112 (1981).
[33]H. Feshbach, Ann. Phys. (N.Y.) **159**, 150 (1985).
[34]D. Wilmore and P. E. Hodgson, Nucl. Phys. **55**, 673 (1964).
[35]F. D. Becchetti and G. W. Greenlees, Phys. Rev. **182**, 1190 (1969).
[36]M. Blann and H. K. Vonach, Phys. Rev. C **28**, 1475 (1983).
[37]W. Scobel, H. H. Bisem, J. Friese, H. Krause, H. J. Langanke, R. Langkau, P. Plischke, and R. Wien, Proceedings of the International Workshop on Reaction Models for Continuous Spectra of Light Particles, (Bad Honnef, 1979), edited by J. Ernst, p. 65.
[38]S. M. Austin, in *Proceedings of the Conference on the* (p,n) *Reaction and the Nucleon-Nucleon Force,* edited by C. D. Goodman *et al.* (Plenum, New York, 1980), p. 203.
[39]W. Dilg, W. Schantl, H. K. Vonach, and M. Uhl, Nucl. Phys. **A217**, 269 (1973).
[40]J. M. Akkermans and H. Gruppelaar, Z. Phys. A **321**, 605 (1985).